Available online at www.sciencedirect.com
SCIENCE DIRECT®
Journal of Catalysis 222 (2004) 80–86
JOURNAL OF CATALYSIS
www.elsevier.com/locate/jcat

# Oxidation activity and $^{18}O$-isotope exchange behavior of nickel oxide-stabilized cubic zirconia

Mohan K. Dongare,[a,*] Kusum Malshe,[a] Chinnakonda S. Gopinath,[a] Irmina Kris Murwani,[b] and Erhard Kemnitz [b]

[a] *Catalysis Division, National Chemical Laboratory, Pune 411008, India*
[b] *Institute for Chemistry, Humboldt University, 12489 Berlin, Germany*

Received 2 July 2003; revised 31 October 2003; accepted 18 November 2003

**Abstract**

A series of NiO–$ZrO_2$ samples with 2 to 40 mol% of NiO were prepared using a sol–gel synthesis technique and calcined at 873 K. XRD characterization of the samples revealed the stabilization of a cubic zirconia- (fluorite) phase containing nickel oxide up to 20 mol%. Bulk NiO characteristics were observed above 20 mol% loading of NiO. The linear decrease in lattice parameter up to 20 mol% of NiO indicates the probable incorporation of $Ni^{2+}$ into the lattice position of $Zr^{4+}$ ions. The NiO–$ZrO_2$ sample with 20% NiO retained its cubic phase even after prolonged heating at 1273 K, indicating 20 mol% as an optimum content of NiO for a thermally stable cubic zirconia phase. The BET surface areas of these samples were in the range of 40 to 70 $m^2\,g^{-1}$. XPS spectra along with XRD data indicated that at low (5 mol%) concentrations of NiO, $Ni^{2+}$ enters $ZrO_2$ lattice substitutionally creating oxygen vacancies. TPR of NiO–$ZrO_2$ showed the reduction of nickel oxide at 533 and 633 K, indicating nickel in two different environments, at a substitutional position and at a surface/interstitial position. $^{18}O$-isotope exchange studies of these samples showed a partial heterogeneous exchange and the $T_{onset}$ was found to be lowest for the sample containing 20 mol% NiO. The activity for $CH_4$ and CO oxidation was investigated by $^{18}O$-isotope exchange as well as catalytic studies in complete oxidation of $CH_4$ and CO. The activity for $CH_4$ oxidation was highest for the NiO–$ZrO_2$ sample with 20 mol% NiO. $CH_4$ and CO oxidation with $^{18}O$ isotope over NiO–$ZrO_2$ catalysts showed the formation of $CO_2$ with $^{16}O$ (amu 44), suggesting that the bulk oxygen is acting as an active species for methane oxidation. The structure of NiO–$ZrO_2$ samples with varying NiO content and its correlation with catalytic activity mechanism is discussed.


*Keywords:* NiO-stabilized zirconia; Methane oxidation; CO oxidation; $^{18}O$-isotope exchange; Sol–gel synthesis

## 1. Introduction

Transition metal oxide-stabilized zirconia has shown reasonably good catalytic activity for complete oxidation of methane as well as for *n*-butane [1,2]. Especially, copper oxide-stabilized zirconia showed an excellent catalytic activity for complete oxidation of methane and carbon monoxide. The catalytic activity was correlated to the high dispersion of copper as an active redox species into the cubic zirconia combined with oxygen mobility due to the oxygen vacancies because of substitution lattice zirconium by copper ions [3]. Ni-supported yttria–zirconia or ceria–zirconia is being widely studied for its applications as a catalyst for steam reforming of methane and methanol [4,5], for partial oxidation of methane [6], and as an anode material in solid oxide fuel cells [7]. Conventionally Ni-supported zirconia catalysts are prepared by the wet impregnation method using a nickel salt solution and yttria-stabilized cubic zirconia as a support which results in a two-phase binary metal oxide catalyst. It is now well established that the catalytic activity of NiO-supported zirconia catalysts is very sensitive to the method of preparation and their subsequent heat treatment. The ultrasonic mist pyrolysis method was found to be useful for the preparation of micrometer-scale NiO/$ZrO_2$ powders, which showed a high efficiency as anodes in SOFC as well as for methane oxidation to CO and $CO_2$ [7]. Ni–Ce–$ZrO_2$ catalysts prepared by a one-step coprecipitation digestion method showed higher activity and stability compared to catalysts by a conventional impregna-

* Corresponding author.
*E-mail address:* dongare@cata.ncl.res.in (M.K. Dongare).

0021-9517/$ – see front matter 
doi:10.1016/j.jcat.2003.11.009

tion method [8]. The higher activity, conversion, and stability of these catalysts were related to the nanocrystalline nature of cubic $Ce_{1-x}Zr_xO_2$ producing a strong interaction with finely dispersed nanosized $NiO_x$ crystallites.

In continuation of our efforts to stabilize zirconia into the cubic phase using transition metal oxides we have synthesized nickel oxide-stabilized zirconia for its use as a catalyst for methane oxidation. Here we report the preparation of $NiO/ZrO_2$ catalyst by the sol–gel technique, which results in $Ni^{2+}$ ions occupying different sites in the stabilized cubic zirconia phase. In this work, the $^{18}O$-exchange process and oxidation of $CH_4$ and CO on $NiO–ZrO_2$ are investigated by online mass spectrometry. The results are compared with those obtained from the catalytic oxidation of methane on $NiO–ZrO_2$.

## 2. Experimental

### 2.1. Preparation of NiO–ZrO$_2$ samples

Samples of Ni-stabilized zirconia were prepared employing the sol–gel technique. A solution of nickel nitrate in isopropanol was added under constant stirring to a solution of zirconium butoxide in butanol. The final homogeneous solution thus formed was allowed to stand for 2–3 h. A transparent greenish gel was formed which was air-dried. The resulting glassy solid was ground to a fine powder and subsequently heat-treated at different temperatures to study the X-ray structure and phase transformations. The samples were heated for 12 h at 623 K, for 12 h at 873 K, and for another 12 h at 1273 K to study the phase transformation.

### 2.2. Catalyst characterization

#### 2.2.1. X-ray diffraction

The powder X-ray diffraction analysis was carried out using a Rigaku X-ray diffractometer (Rigaku miniflex) equipped with a Ni-filtered Cu-$K_\alpha$ (1.542 Å) radiation and a graphite crystal monochromator. Silicon was used as an external standard. The data were collected in the $2\theta$ range, 20–80° with a step size of 0.02° $2\theta$ and counting time of 15 s at each step. The observed inter planar '*d*' spacing was corrected with respect to silicon. The unit cell parameters were determined using the corrected *d* values.

#### 2.2.2. X-ray photoelectron spectroscopy

Photoemission spectra were recorded on a VG Microtech Multilab ESCA 3000 spectrometer using a nonmonochromatized Mg-$K_\alpha$ X-ray source ($h\nu = 1253.6$ eV). Base pressure in the analysis chamber was maintained at the 3–6 $\times$ $10^{-10}$ Torr range. The energy resolution of the spectrometer was set at 0.8 eV with Mg-$K_\alpha$ radiation at a pass energy of 20 eV. Binding energy (BE) calibration was performed with a Au $4f_{7/2}$ core level at 83.9 eV. BE of adventitious carbon (284.9 eV) was utilized for charge correction with all the samples. The error in all the BE values reported here is within $\pm 0.1$ eV.

#### 2.2.3. Temperature-programmed reduction

Temperature-programmed reduction was performed in a quartz tube reactor and hydrogen consumption was measured by a TCD detector. A weighed amount (25 mg) of the sample was placed in the reactor and treated in 10% $O_2$/He gas mixture at 573 K for 30 min and cooled down to 373 K in the same atmosphere; then 20 ml/min of the 1% $H_2$/Ar gas mixture was allowed to flow through the reactor. The temperature was increased to 1073 K at a heating rate of 10 K/min.

The surface areas (BET) of the samples were determined after degassing the samples at 573 K and analyzing the $N_2$ adsorption isotherm at liquid nitrogen temperature (ASAP 2000 system, Micromeritics).

#### 2.2.4. Temperature-programmed $^{18}O$-isotope exchange and oxidation measurements

Temperature-programmed $^{18}O$-isotope exchange and oxidation measurements were carried out in a quartz reactor with an online-coupled mass spectrometer. Before starting the reaction, about 300 mg of the sample was heated for 4 h at 573 K and 200 Pa, in order to remove $H_2O$, $CO_2$, and other molecules from the surface of the oxide. After cooling down to room temperature, Ar, $^{18}O_2$, and the second reactant (viz. $^{16}O_2$, CO, or $CH_4$) were introduced in an appropriate ratio into the reaction system. The initial pressure was adjusted to $p_0 = 100$ Pa and the quartz reactor was heated to 973 K applying a constant heating rate of $\beta = 10\ \mathrm{K\,min^{-1}}$. The variation of the gas-phase composition during constant heating was analyzed by a quadrupole mass spectrometer (QMG421I, Pfeiffer Vacuum GmbH). During the interaction among $^{18}O_2$, $^{16}O_2$, and the solid oxide, diffusion, sorption, and $^{18}O$-isotope exchange processes may take place according to the following scheme (Eqs. (1)–(3)).

*Homomolecular $^{18}O$-isotope exchange*

$$^{18}O_{2(g)} + {}^{16}O_{2(g)} \rightarrow 2\,{}^{16}O\,{}^{18}O_{(g)}; \tag{1}$$

*Partially heteromolecular $^{18}O$-isotope exchange*

$$^{18}O_{2(g)} + {}^{16}O_{(s)} \rightarrow {}^{16}O\,{}^{18}O_{(g)} + {}^{18}O_{(s)}; \tag{2}$$

*Completely heteromolecular $^{18}O$-isotope exchange*

$$^{18}O_{2(g)} + 2\,{}^{16}O_{(s)} \rightarrow {}^{16}O_{2(g)} + 2\,{}^{18}O_{(s)}. \tag{3}$$

From the occurrence of the individual processes and the onset temperatures, conclusions can be drawn on the temperature regions of enhanced oxygen mobility and activity to promote homomolecular or heteromolecular redox reactions. The measuring principle and the theoretical background of the $^{18}O$-isotope exchange measurements were described in detail elsewhere [9,10]. In a similar manner, the oxidation of CO or $CH_4$ by $^{18}O_2$ can be investigated. For that purpose, the reaction gas mixture ($p_0 = 100$ Pa) was introduced into the quartz finger and the reaction system was

heated to 873 K. The onset of the oxidation reaction and the oxidation product distribution were determined to draw conclusions on the mechanism of the catalytic process.

*2.2.5. Catalytic oxidation of $CH_4$*

The catalytic oxidation of $CH_4$ was performed in an upflow, fixed-bed quartz reactor. Approximately 300 mg of the ground oxide was pressed in the form of pellet. The pellet was crushed to obtain the catalyst in the form granules (mesh size 0.5–1 mm) and was preheated for 1 h at 723 K in $N_2$ flow (10 ml $min^{-1}$). After cooling down to 523 K, the sample was exposed to the reaction gas mixture of $O_2$ (48 ml $min^{-1}$) and $CH_4$ (12 ml $min^{-1}$) at atmospheric pressure and at the residence time of 0.25 s (gas hourly space velocity GHSV of 15,000 $h^{-1}$). After 20 min, the gas composition at the reactor exit was determined by an online gas chromatograph (Shimadzu 17A) with thermal-conductivity detector (column, C molecular sieve, i.d. 3 mm, length, 2 m). The conversion of methane was calculated in terms of $CO_2$ formed. The catalyst was tested with ascending and descending temperature to study the light-off temperature and catalyst deactivation. The catalytic activity was also studied at various lower residence times to study the mass-transfer limitations. Similarly few samples of catalyst were also tested for CO oxidation in the absence and in the presence of hydrogen to test its utility for removal of CO from hydrogen produced by steam reforming for a polymer membrane fuel cell.

## 3. Results and discussion

### *3.1. Catalyst characterization*

X-ray diffraction patterns of various NiO–$ZrO_2$ compositions calcined at 873 K are shown in Fig. 1. Results show that adding NiO to $ZrO_2$ using the sol–gel technique results in a single-phase composition with a cubic (Fluorite) structure up to 20 mol% NiO. Compositions with concentration of NiO above 20 mol% show distinct NiO reflections ($2\theta = 37.3$, 43.4, 61.6) and indicate its presence as a second phase. The variation of lattice constant of cubic phase is shown in Fig. 2. Up to 20 mol% NiO, a linear decrease in lattice constant with increase in the concentration of NiO most likely indicates that nickel enters the lattice of zirconia substitutionally. Smaller size $Ni^{2+}$ (ionic radius 0.78 Å) replaces bigger size $Zr^{4+}$ (0.87 Å) and hence reduction in lattice constant is expected. However, the extent of decrease is much smaller than when all the $Ni^{2+}$ occupies a substitutional position. This behavior is similar to the one reported for $Cu^{2+}$ substitution of $Zr^{4+}$ [3]. It is therefore suggested that part of the $Ni^{2+}$ may enter the $ZrO_2$ lattice interstitially.

Thermal stability of the samples was also studied. X-ray diffraction patterns of these samples calcined at 1273 K are shown in Fig. 3. It is interesting to note that, like pure zirconia, samples with NiO concentrations upto 15 mol% also

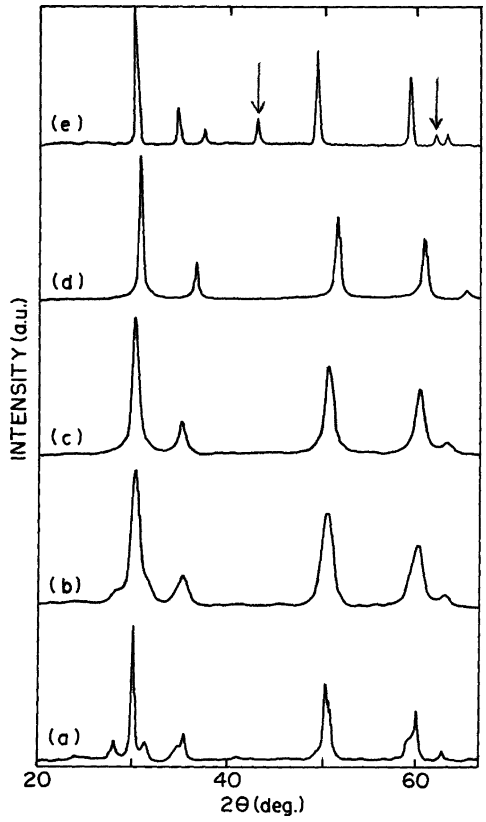


Fig. 1. X-ray diffraction patterns of (a) pure $ZrO_2$, $ZrO_2$ with (b) 2% NiO, (c) 10% NiO, (d) 20% NiO, and (e) 25% NiO. Arrows indicate the NiO peaks.

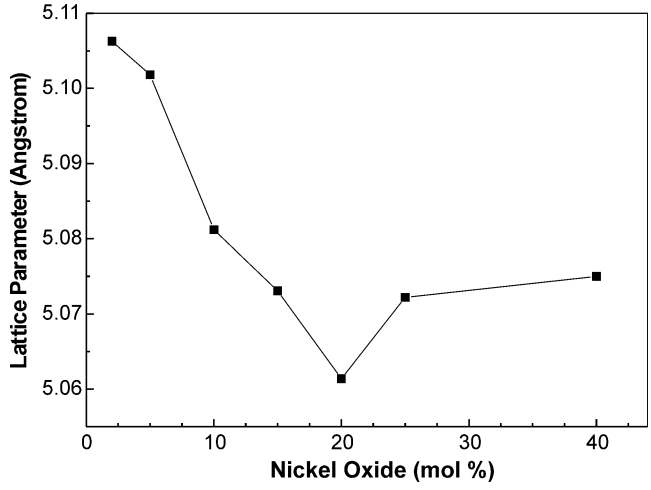


Fig. 2. Variation of lattice constant as a function of NiO concentration.

transform to monoclinic structure ($2\theta = 28.32$ and 31.6) at high temperature. However, with 20–25 mol% NiO, the cubic structure is maintained even at high temperatures, indicating that 20 mol% NiO is required to obtain thermally stable cubic zirconia similar to CaO or $Y_2O_3$-stabilized zirconia.

A Ni $2p_{3/2}$ core-level spectrum is shown for all samples in Fig. 4 (top panel). At a low input of NiO (at 2mol%), only

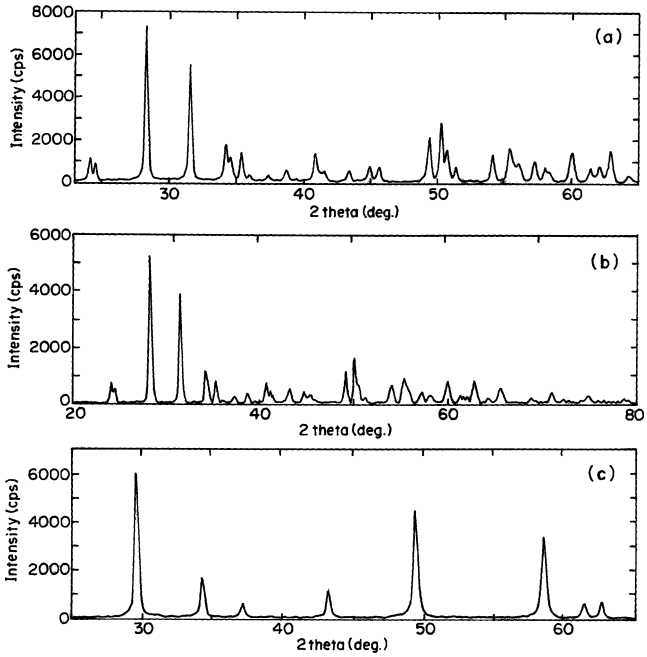


Fig. 3. X-ray diffraction patterns of $ZrO_2$ with (a) 10% NiO, (b) 15% NiO, and (c) 20% NiO after calcination at 1273 K.

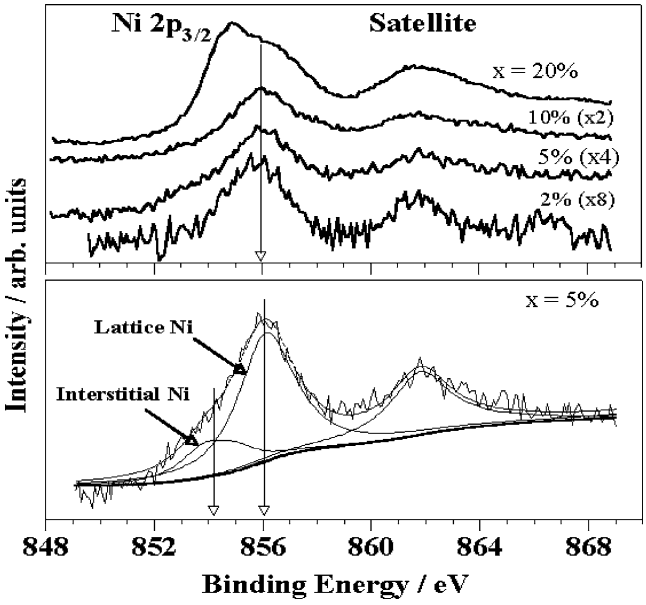


Fig. 4. Ni $2p_{3/2}$ core-level XPS of representative NiO–$ZrO_2$ samples shown in top panel. Bottom panel shows 5% NiO-loaded spectrum after deconvolution to show the lattice and interstitial Ni in $ZrO_2$ substrate.

one peak appears at a binding energy of 856 eV. However, at intermediate NiO concentration (5 and 10 mol%) a shoulder appears at a lower BE (854 eV) in addition to the above peak at 856 eV. At high input of NiO (20 mol%) the Ni $2p_{3/2}$ peak structure is entirely different and very much similar to that of bulk NiO [11]. It is concluded from the above observation that all $Ni^{2+}$ ions occupy the lattice position in $ZrO_2$ below 5 mol%. Above 5 mol%, a small amount of Ni ions occupies the interstitial position and the remaining goes to

Table 1
Physicochemical characterization of NiO–$ZrO_2$ for representative samples

| NiO (mol%) | XRD phase | Lattice parameter ($a$) (Å) | Surface area $S_{BET}$ ($m^2\,g^{-1}$) | Ni/Zr surface atomic ratio from XPS |
|---|---|---|---|---|
| 0.00 | Cubic $ZrO_2$ + monoclinic (traces) | 5.110 | 40 | – |
| 2.00 | Cubic $ZrO_2$ | 5.106 | 51 | 0.02 |
| 5.00 | Cubic $ZrO_2$ | 5.101 | 65 | 0.08 |
| 10.00 | Cubic $ZrO_2$ | 5.082 | 62 | 0.19 |
| 15.00 | Cubic $ZrO_2$ | 5.073 | 66 | – |
| 20.00 | Cubic $ZrO_2$ | 5.061 | 70 | 3.03 |
| 25.00 | Cubic $ZrO_2$ + NiO (traces) | 5.072 | 55 | – |
| 40.00 | Cubic $ZrO_2$ + NiO | 5.075 | 45 | – |

the lattice positions. The intensity and BE of Ni species that are at interstitial positions is clearly shown in the bottom panel in Fig. 4 after deconvolution. Similar characteristics of bulk NiO appeared at high input of NiO, clearly demonstrating that $ZrO_2$ is covered mostly by NiO. This is further supported by a high Ni/Zr ratio for 20 mol% NiO sample calculated from Ni $2p_{3/2}$ and Zr $3d_{5/2}$ peaks (Table 1). At low Ni input the above ratio is close to the bulk value and that indicates the uniform distribution of Ni in the $ZrO_2$ lattice. The above results clearly support the results obtained from XRD.

Fig. 5 shows the photoemission results from O 1s core level up to a NiO input level of 10 mol%. A main peak is observed around 530 eV for all compositions. Additionally, there is a shoulder seen between 531.3 and 532 eV (indicated by arrow) for all the samples and its intensity increases with NiO input. The main peak at 530 eV is attributed to the oxygen in the zirconia lattice and the high BE shoulder is attributed to the oxygen vacancies and/or $O^-$ species associated with Ni. BE of the latter species increases with NiO input and indicates an increase in its concentration. This ob-

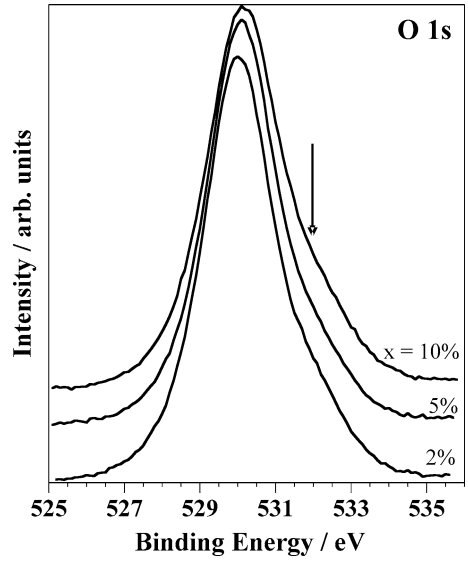


Fig. 5. XPS of O 1s core level of NiO–$ZrO_2$ samples.

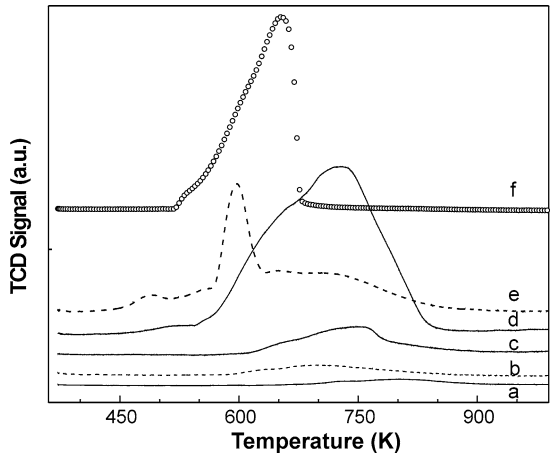


Fig. 6. Temperature-programmed reduction of (a) 2% $NiO/ZrO_2$, (b) 5% $NiO/ZrO_2$, (c) 10% $NiO/ZrO_2$, (d) 20% $NiO/ZrO_2$, (e) 40% $NiO/ZrO_2$, and (f) bulk NiO. Bulk NiO intensity is divided by a factor of 5.

servation hints that high oxygen mobility might be expected in this material, which will directly influence the catalytic properties, especially oxidation, in a significant way.

TPR of pure NiO showed only one reduction peak at 656 K, indicating reduction of $Ni^{2+}$ to $Ni^0$ without going through intermediate oxide. TPR results of a series of $NiO/ZrO_2$ samples and bulk NiO are shown in Fig. 6. NiO–$ZrO_2$ sample containing 2 mol% NiO (Fig. 6, a) shows two reduction peaks in the temperature range of 703–733 and 773–853 K, suggesting that NiO in zirconia is in two different environments. The reduction peak at 802 K may be assigned to the $Ni^{2+}$ in the substitutional lattice position with a stronger interaction with lattice. The peak at 733 K may be due to the highly dispersed NiO on the zirconia surface, requiring a higher temperature for reduction than pure NiO because of a metal support interaction. As the NiO content in the zirconia is increased the intensity (Fig. 6, b, c, d) of both peaks keeps on increasing and NiO–$ZrO_2$ with 20 mol% showed the maximum peak intensity for both peaks. A strong peak in the temperature range of 573–623 and a small hump in the range of 673–773 K for the NiO–$ZrO_2$ sample with 40 mol% NiO suggest a maximum amount of NiO on the surface as bulk nickel oxide. These TPR results are in good agreement with the XRD results where above 20 mol% a separate NiO phase starts appearing. Takeguchi et al. [5] prepared high-surface zirconia, NiO–$CeO_2$–$ZrO_2$ catalysts by a glycothermal method and the TPR results showing two reduction temperatures were correlated to two types of NiO with different particle sizes and their interaction to the support.

### 3.2. Methane oxidation

The catalytic activity of NiO–$ZrO_2$ samples was studied after the ground powder was calcined at 873 K. Fig. 7 shows the results of catalytic activity of various NiO–$ZrO_2$ samples between 523 and 823 K. All the samples were found to be active and total conversion of $CH_4$ to $CO_2$ was observed

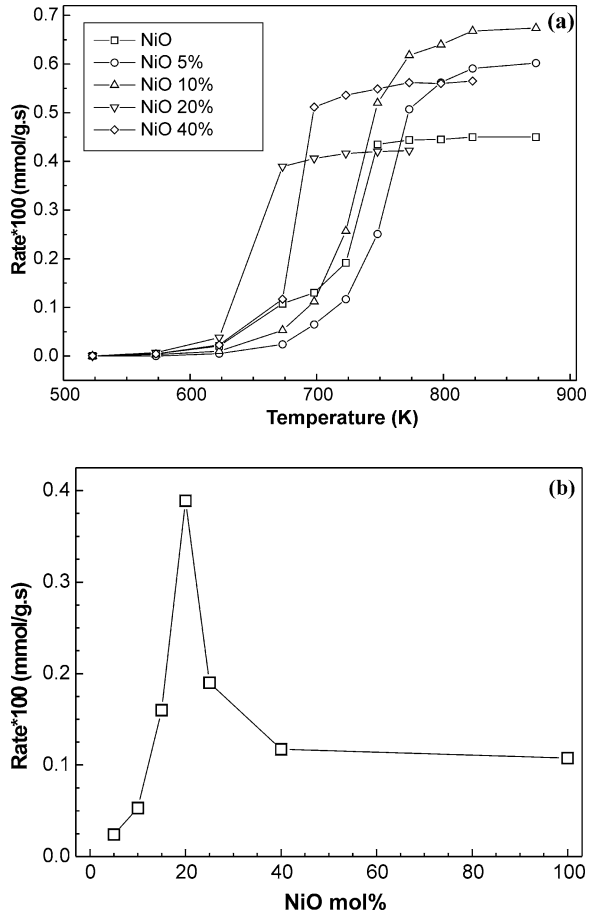


Fig. 7. (a) Kinetics of methane oxidation to $CO_2$ on NiO–$ZrO_2$ samples are given. (b) Rate of $CO_2$ formation at 673 K is plotted for all NiO loadings.

between 723 and 823 K. It was observed that the light-off temperature shifts toward the lower side with the addition of nickel to $ZrO_2$. The presence of $CO_2$ and the absence of CO in the oxidation product confirms the complete oxidation of methane. The temperature range between appreciable methane conversion and complete conversion was always less than 100 K. This may be associated to the autothermal oxidation due to the exothermic nature of the reaction.

A sample containing 20 mol% NiO showed the best catalytic performance with almost complete conversion at 673 K. An increase in catalytic activity with an increase in Ni content shows that the catalytic activity is linked to the Ni species in the lattice as well as on the surface. But the sample containing 40 mol% NiO shows lesser activity as compared to the 20 mol% sample. This may be because of the fact that at such a high concentration of nickel species, the catalyst starts to behave like the bulk nickel oxide.

### 3.3. CO oxidation

The results of CO oxidation with 10 mol% NiO and 20 mol% $NiO/ZrO_2$ are shown in Fig. 8. It is seen that CO is oxidized to $CO_2$ below 383 K for the 20 mol% NiO which is nearly 50 K lower than (433 K) required for the 10 mol%

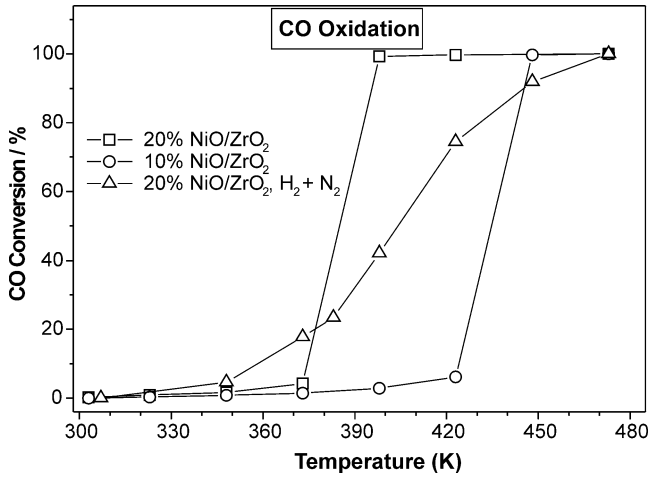


Fig. 8. CO oxidation with 10% NiO, 20% NiO/$ZrO_2$, and 20% NiO/$ZrO_2$ in presence of 1% hydrogen.

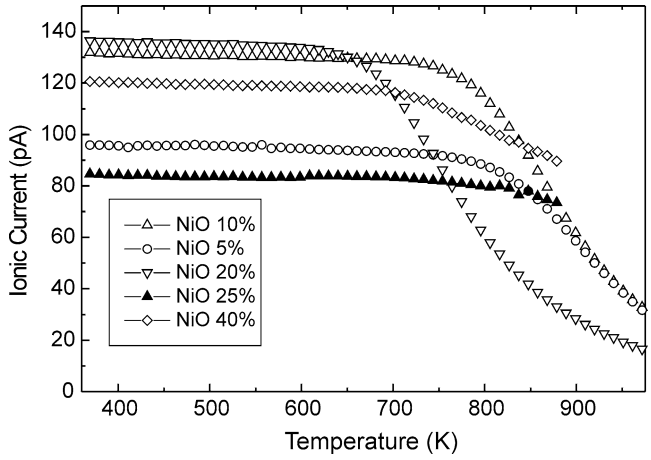


Fig. 9. $^{18}O$-isotope exchange interaction with $ZrO_2$ containing 5% NiO, 10% NiO, 20% NiO, 25% NiO, and 40% NiO.

NiO sample. These results are in agreement with the results obtained in methane oxidation. As expected among the two samples studied the 20 mol% NiO/$ZrO_2$ was found to be the more active sample for CO oxidation. When CO oxidation was carried out in presence of hydrogen (1% CO, 76% $H_2$, 2% $O_2$, and remaining $N_2$), CO was completely oxidized to $CO_2$. The catalytic activity was tested for five cycles without any decrease in catalytic activity, indicating the utility of this catalyst for purification of hydrogen (CO removal) produced from steam reforming of methanol for polymer membrane fuel cells.

### 3.4. Isotope exchange

Temperature-programmed $^{18}O$-isotope exchange measurements of the samples were carried out to investigate the oxygen transfer mechanism for these catalysts. The results of the $^{18}O$-isotope exchange reaction of NiO–$ZrO_2$ catalysts are illustrated in Fig. 9. In the temperature range of 373–598 K, all the ionic currents of $^{16}O_2$, $^{18}O_2$, and $^{16}O\,^{18}O$ are constant. The sample containing 20 mol% NiO showed the lowest $T_{onset}$ for the change of the oxygen ionic currents. At about 598 K, $^{18}O_2$ begins to decrease and continues up to 973 K. At the same time, the $^{16}O_2$ and $^{16}O\,^{18}O$ ionic currents increase. But the rates of increase or decrease are different depending on the temperature range. The $^{18}O_2$ decreases with reaction temperature demonstrating completely heteromolecular $^{18}O$-isotope exchange and reaches a minimum at 923 K. The partially heteromolecular $^{18}O$-isotope exchange simultaneously takes place between 673 and 973 K.

During $^{18}O$-isotope exchange measurements on all samples of NiO–$ZrO_2$, considerable quantities of $^{16}O\,^{18}O$ were formed by partial heteromolecular $^{18}O$-isotope exchange. Moreover, the formation of $^{16}O\,^{18}O$ reaches a maximum for the samples with NiO content between 5 and 20 mol%; above 20 mol% the formation rate of $^{16}O\,^{18}O$ increases without a maximum. The similar tendency is also observed for $^{16}O_2$. This shows that the samples with NiO content more than 20% no longer incorporate Ni in the lattice of $ZrO_2$, and this NiO is the source of a higher $^{16}O$ release. This is in agreement with TPR and XRD results where above 20 mol% a separate NiO phase starts to appear.

### 3.5. The reaction of $^{18}O_2$ and $CH_4$ under static conditions

In the above section, the $^{18}O_2$-isotope exchange behavior of the samples was investigated. In order to understand and confirm the reaction mechanism, oxidation of methane with $^{18}O_2$ isotope gas was performed as described above in the same apparatus.

Fig. 10 depicts the temperature dependence of the ionic currents of the reactant and the products over the most active 20 mol% NiO catalyst. Consumption of $CH_4$ resulted in the formation of $C\,^{16}O_2$, with traces of $C\,^{16}O\,^{18}O$ and almost no $C\,^{18}O_2$. Considering the ratio of $^{18}O$ which is the only oxygen source in the original gas phase in the oxidation products, one can deduce that the oxidizing agent in the reaction is the metal in a high oxidation state and the oxygen being transferred into the gaseous products from the solid. Hence, a possible reaction pathway can be summarized as follows:

$$CH_{4(ad)} + 4\,{}^{16}O^{2-}_{(s)} \rightarrow C\,{}^{16}O_{2(g)} + 2H_2\,{}^{16}O_{(g)} + 8e^-,$$

$$8/n\,Ni^{2+}_{(s)} + 8e^- \rightarrow 8/n\,Ni^{(2-n)+}_{(s)},$$

$$8/n\,Ni^{(2-n)+}_{(s)} + 2\,{}^{18}O_2(g) \rightarrow 8/n\,Ni^{2+} + 4\,{}^{18}O^{2-}_{(s)}.$$

Such a redox mechanism in which the solid oxide phase is directly involved is normal for transition metal oxide catalysts [12,13]. As the oxygen in the products originates from the solid surface containing $^{16}O^{2-}$ only at the beginning, far more $C\,^{16}O_2$ is produced than $C\,^{16}O\,^{18}O$ and $C\,^{18}O_2$. With longer reaction times, more and more $^{18}O$ is incorporated into the solid via the above-noted mechanism and complete heteromolecular isotope exchange. This leads to a gradual increase in the ionic current of $C\,^{16}O\,^{18}O$.

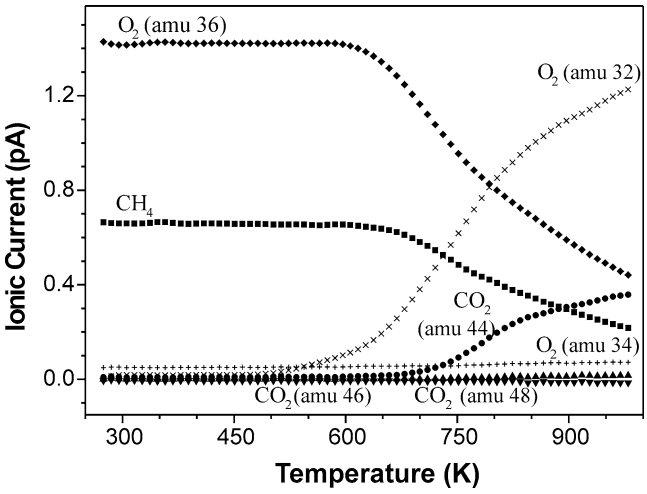


Fig. 10. Methane oxidation by $^{18}O_2$ on cubic 20 mol% NiO–$ZrO_2$.

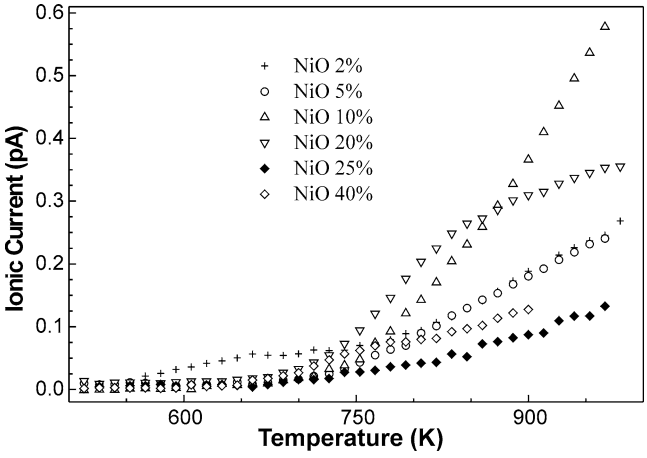


Fig. 11. Oxidation of methane to $CO_2$ (amu 44) by $^{18}O_2$ on NiO/$ZrO_2$ catalysts.

Fig. 11 shows the formation of C $^{16}O_2$ during the oxidation reaction over different samples. The catalytic activities observed here are consistent with the results obtained by flow reaction. The most active catalyst, 20 mol% NiO also displays the highest activity in isotope exchange. Clearly, a high mobility of oxygen species leads to high oxidation activity. It is generally considered that for complete oxidation catalysts, considerable amounts of weakly bound oxygen are required on the surface and the weaker the oxygen bonding with the catalyst surface, the more efficient the catalyst for complete oxidation as in the present case [13]. However, very weakly bound oxygen leads to very high oxygen release and a lowering of the surface reoxidizability. This causes a decrease in the catalytic oxidation activity [13].

## 4. Conclusions

NiO/$ZrO_2$ containing 2–40 mol% NiO prepared by the sol–gel technique showed the formation of single-phase cubic (fluorite type) zirconia upto 20 mol% of NiO. Above 20 mol%, a second bulk NiO phase is formed along with cubic zirconia. Up to 20 mol% NiO, part of Ni is incorporated in the zirconia lattice at a substitutional position and part remains on the surface and in the interstitial positions. Among the series, NiO/$ZrO_2$ containing 20 mol% NiO was found to be the most active catalyst for methane and CO oxidation. $^{18}$Oxygen isotope exchange study revealed heteromolecular exchange and the methane oxidation using $^{18}$oxygen isotope clearly indicated the lattice oxygen as the active $O^-$ species in methane oxidation. The presence of Ni at a substitutional site creates oxygen vacancies. Higher oxygen mobility as well as the ease of reduction and oxidation of Ni leads to higher catalytic activity of NiO/$ZrO_2$ for methane and CO oxidation.

## References

[1] A. Keshavaraja, A.V. Ramaswamy, Appl. Catal. B 8 (1996) L1.
[2] V.R. Chaudhary, B.S. Upadhe, S.G. Pataskar, A. Keshawaraja, Angew. Chem. 108 (1996) 2538.
[3] M.K. Dongare, V. Ramaswamy, C.S. Gopinath, A.V. Ramaswamy, S. Scheurell, M. Brueckner, E. Kemnitz, J. Catal. 199 (2001) 209.
[4] W.S. Dong, H.S. Roh, K.W. Jun, S.E. Park, Y.S. Oh, Appl. Catal. A 226 (2002) 63.
[5] T. Takeguchi, S.N. Furukawa, M. Inoue, J. Catal. 202 (2001) 14.
[6] A.M. Dikkim, Catal. Today 46 (1998) 147.
[7] A.S. Carrillo, T. Tagawa, S. Goto, Mater. Res. Bull. 36 (2001) 1017.
[8] H.S. Potdar, H.S. Roh, K.-W. Jun, M.L. Ji, W. Zhong, Catal. Lett. 84 (2002) 95.
[9] E. Kemnitz, A.A. Galkin, T. Olesh, S. Scheurell, A.P. Mozhaev, G.N. Mazo, J. Therm. Anal. 48 (1997) 997.
[10] E. Kemnitz, D.H. Menz, C. Stocker, T. Olesh, Thermochim. Acta 225 (1993) 119.
[11] L. Sangaletti, L.E. Depero, F. Parmigiani, Solid State Commun. 103 (1999) 421.
[12] V.D. Sokolovskii, Catal. Rev.-Sci. Eng. 32 (1990) 1.
[13] N. Yamazoe, Y. Teraoka, Catal. Today 8 (1990) 175.